

# *On the nature of intraplate earthquakes*

**Pradeep Talwani**

**Journal of Seismology**

ISSN 1383-4649

J Seismol

DOI 10.1007/s10950-016-9582-8



 Springer

**Your article is protected by copyright and all rights are held exclusively by Springer Science +Business Media Dordrecht. This e-offprint is for personal use only and shall not be self-archived in electronic repositories. If you wish to self-archive your article, please use the accepted manuscript version for posting on your own website. You may further deposit the accepted manuscript version in any repository, provided it is only made publicly available 12 months after official publication or later and provided acknowledgement is given to the original source of publication and a link is inserted to the published article on Springer's website. The link must be accompanied by the following text: "The final publication is available at [link.springer.com](http://link.springer.com)".**



# On the nature of intraplate earthquakes

Pradeep Talwani

Received: 11 November 2015 / Accepted: 22 April 2016  
© Springer Science+Business Media Dordrecht 2016

**Abstract** Continental intraplate regions are characterized by uniform stresses over thousands of kilometers. Local stresses, with wavelengths of tens to hundreds of kilometers can accumulate at inhomogeneities lying within these regional fields. A variety of geological structures, herein called local stress concentrators (LSCs), act as elastic inhomogeneities. The temporal buildup of stress depends on the particular structure and its geometrical relationship with the regional stress field. The interaction of the local and the regional stress fields can result in the rotation of the latter over wavelengths of tens to hundreds of kilometers. This rotation can be detected by direct measurement or from seismicity data. Intraplate earthquakes (IPEs) result when the local stresses become comparable with their regional counterparts, i.e., hundreds of megapascals. Globally, most of the seismic energy release associated with IPEs occurs within old rifts which contain LSCs most favorable for stress buildup by stress inversion. Of the various LSCs, stepover en echelon faults are associated the largest IPEs. In low tectonic strain rate regions, IPEs are associated with larger stress drops. With the availability of a variety of LSCs, there is generally an absence of repeat earthquakes. Instead, successive earthquakes occur on different structures, leading to the observation of “roaming” earthquakes. These observations suggest a need for a reevaluation of seismic hazard

estimation techniques. This study addresses some of these facets of the nature of IPEs with global examples, including a unique, detailed seismicity and geodetic data set collected in a dozen years following the 2001 M 7.7 Bhuj earthquake in western India.

**Keywords** Intraplate Earthquakes · Local stress concentrators · Stress field rotation · Seismic hazards

## 1 Introduction

Although continental intraplate earthquakes are infrequent, scattered spatially, and account for a very small fraction of the global seismic energy release, they cause a disproportionate amount of damage. Because of their rarity, efforts to study them have been limited. As the results of those efforts began to accumulate, several common features were recognized and used to study their nature. Albeit intraplate earthquakes also occur within oceanic plates, this study is focused exclusively at understanding the nature of continental intraplate earthquakes (IPEs).

An inventory of  $M \geq 4.5$  intraplate earthquakes showed that they are preferentially located in old rift structures and at boundaries of cratons (Mooney et al. 2012; Talwani 2014; and references therein). Of these, most of the seismic energy release is associated with rifts (Schulte and Mooney 2005); possibly because among different types of intraplate discontinuities, rifts with strongly thinned crust appear to be prone to early

---

P. Talwani (✉)  
Department of Earth and Ocean Sciences, University of South  
Carolina, 700 Sumter Street, Columbia, SC 29208, USA  
e-mail: ptalwani@geol.sc.edu

inversion in response to collision-related intraplate stresses (Ziegler 1987; Hansen and Nielsen 2003).

Recent studies have now begun to address the details of crustal structure associated with IPEs on craton boundaries in Brazil (Agurto-Detzel et al. 2015) and the Eastern Tennessee seismic zone (Powell et al. 2014; Powell 2015). In this study, the focus will be on rift-related IPEs.

The preferential location of IPEs within rifts suggests that their locations are not random but have a solid mechanical basis. Although the mechanics of the rupture process of an earthquake in an intraplate or a plate boundary setting is the same, ascribing a physical basis to explain the primary process(es) responsible for the genesis of an intraplate event has remained one of the unresolved problems of seismology.

As most of the larger IPEs are rift related, they have been the focus of studies seeking the mechanical cause for their genesis. To explain their occurrence, early ideas fell into two general types of models. In the first, untestable models, the localizing structures were assumed to be close to failure and a small stress perturbation, due to a regional stress source, triggered the earthquake. Among the variety of possible sources for this perturbation are erosion or deposition at the surface (e.g., Haxby and Turcotte 1976; Calais et al. 2010), glacial isostatic adjustment (e.g., Stein et al. 1979; Zoback 1992), or by stress transfer to the brittle upper crust (Liu and Zoback 1997; Kenner and Segall 2000; Pollitz et al. 2001; Sandiford and Egholm 2008). These models do not address the basic cause of the stress buildup that brought the structure close to failure. The second class of models were developed on the basis of observed spatial association of IPEs with identifiable geologic features, e.g., with buried plutons (Long 1976), fault bends and intersections (King 1986; Talwani 1988), and buried rift pillows (Zoback and Richardson 1996).

Talwani (2014) presented a review of the earlier observations and models, and then integrated them to propose a new model—a unified model for rift-related IPEs, hereafter referred to as the unified model. The basic idea of this model is that there is a stress buildup at suitable geological features, which we refer to as Local Stress Concentrators (LSCs) in response to a uniform far-field regional stress field, associated with plate margin forces. When the magnitude of this local stress buildup

is comparable with the regional stress, it can lead to seismicity, the intraplate earthquakes. This model explains how stresses build up on various geological features and many of their observed characteristics. This model is an initial step in providing a framework for studying the genesis of IPEs.

As a next step, complementary observations aimed at improving our understanding of the nature of IPEs within the framework of the unified model are presented in this study. Starting with a summary of the model (next section), the under-recognized role of restraining stepovers as the most notable LSCs associated with IPEs is presented in Sect. 3.

As shown originally by Zoback (1992), and confirmed by the smoothed World Stress Map data, in intraplate regions, long wave-length stress patterns (>2000 km) of the maximum compressive horizontal stress orientation are interrupted by shorter spatial wave-length variations of less than 200 km (Heidbach et al. 2010; Reiter et al. 2014). Zoback (1992) attributed this deviation of the regional stress field as being due to its interaction with stresses associated with some major geologic features.

With the inversion of improved seismicity data, it is now possible to determine the direction of small pockets of stresses associated with LSCs. Talwani (2014) presented examples of statistically significant, >15°, local stress rotation of the regional stress field associated with LSCs with spatial wavelengths of ~tens to hundreds of kilometers. Where the local geological and stress conditions are known, and based on the premises of the unified model, it is now possible to explain these small-scale (~10 km) rotations of stress field. Two examples of the observed local rotations of the stress fields in the St. Lawrence and New Madrid seismic zones are analyzed in Sect. 4. Those rotations were observed long after the main shocks at these locations (1925, St. Lawrence; and 1811–1812, New Madrid) and are not artifacts of co-seismic stress perturbations.

Analyzing detailed anecdotal Chinese historical data, going back ~2000 years, Liu et al. (2011, 2014) observed that large earthquakes (M 6) did not recur at previous epicenters, unlike their plate boundary counterparts, but “roamed” around. Examination of other locations of IPEs with improved spatio-temporal data shows that this phenomenon of “roaming” or non-repeat earthquakes may also be present at lower magnitude levels. Some examples of non-repeat earthquakes are presented in Sect. 5 and may have major implications in

assessing the seismic hazards in low tectonic strain intraplate regions.

Excellent multidisciplinary data have been acquired and continue to be acquired following the M 7.7, 2001 Bhuj earthquake in western India (see Rastogi et al. 2014 for a review). These detailed geodetic and seismicity data are especially useful in understanding the genesis of IPEs and in comparing them with the expectation of the unified model—the observation of local pockets of elevated strain rates in the vicinity of LSCs. A unique set of InSAR data in the region surrounding the epicentral area of the 2001 earthquake provided such an opportunity. A comparison of these data with the local seismicity is presented in Sect. 6. The conclusions of this study are presented in the final section.

**Nomenclature** In a seminal study, Mary Lou Zoback (1992) identified two orders of stress in the continental lithosphere. The first-order mid-plate stress field, extending uniformly over thousands of kilometers, is associated with plate tectonic forces. Ziegler (1987) showed that collision-related major stresses can be transmitted over great distances through continental and oceanic lithosphere. This continental stress is generally compressional with one or both horizontal stress ( $S_{Hmax}$  and  $S_{Hmin}$ ) greater than the vertical stress,  $S_v$ . Superposed on the regional stresses are second-order stress fields with wave lengths of hundreds of kilometers associated with specific geologic and tectonic features. In this study, we will refer to the maximum horizontal stress components of the regional stress, perturbing local stress, and final observed stress as  $S_T$ ,  $S_L$ , and  $S_F$ , respectively.

## 2 Unified model for intraplate earthquakes

Talwani (2014) presented the details of the development and characteristics of this model, which attempted to unify earlier observations and ideas about the subject. The important elements of the model are repeated here in order to provide the background against which various observations in subsequent sections are addressed.

### 2.1 Weak zone models

Starting with the earliest models to explain IPEs, the emphasis was on the presence of preexisting zones of

weakness in the continental crust where they occurred (see, e.g., Sykes 1978). From elasticity theory (e.g., Jaeger and Cook 1979), a far-field stress is concentrated by a heterogeneity with a different elastic modulus. The presence of weak zones in the lower crust and upper mantle, have been suggested as locations where stresses buildup (i.e. act as regional stress concentrators), and can be transferred to shallow crustal faults (see, e.g., Iio et al. 2004).

Using improved seismicity and geodetic data in eastern North America, Mazzotti (2007) presented four geodynamic models to explain their cause, continuing the weak zone theme. He suggested that weak zones in the crust and/or the upper mantle control the intraplate seismicity and emphasized on the mechanical strength of these zones as providing the main constraint on earthquake locations. Currently, we lack direct observational evidence of weak zones and their linkage with the observed seismicity. The assumptions of weak zones (low coefficients of friction and elevated fluid pressures) has been questioned by Hurd and Zoback (2012a, b) who suggest a normal coefficient of friction (0.6–0.8) and hydrostatic pore pressures at these locations.

However, two recent examples have provided observational evidence of such weak zones. To explain the 2004 and 2007 M 6+ earthquakes in the intraplate Niigata-Kobe tectonic zone, Kato (2014) suggested that ductile creeping of a weak lower crust could cause stress loading into seismogenic faults. Seismic tomography and wideband magnetotelluric anomalies beneath the source of the 2004 earthquake were interpreted by Kato (2014) to represent crustal fluids in the vicinity of a dense rift pillow. A similar interpretation, based on detailed seismic tomography, of fluid filled fractures surrounding a rift pillow, was made for the hypocentral zone of the 2001 M 7.7 Bhuj earthquake (Rastogi et al. 2014). The role of fluids in lowering the strength of rocks in both the upper and lower crust, in the earthquake process has long been recognized (e.g., Hickman et al. 1995)

### 2.2 Local stress concentrators

However, the present study does not address weak zones that act as *regional* stress concentrators. We concentrate on stress concentrators that are *local* (with wavelengths of tens to hundreds of kilometers) and have demonstrable association with geological structures. Stresses accumulate at these local stress concentrators (LSCs) in

response to  $S_T$ . Restraining stepovers, fault bends, intersecting faults, shallow plutons, and rift pillows have been known for a long time as locations where stresses accumulate in response to  $S_T$ , i.e., act as LSCs (see Talwani 2014 for a review), and are the focus of this study.

### 2.3 The unified model for intraplate earthquakes

IPEs occur in continental regions characterized by a uniform compressional stress field,  $S_T$ , which extends over thousands of kilometers (Zoback 1992). There is a global pattern of seismic energy release by IPE in response to  $S_T$ . IPEs with  $M \geq 4.5$ , preferentially occurs in failed (or interior) rifts and on passive (or rifted) margins (see, e.g., Johnston and Kanter 1990; Schulte and Mooney 2005). Most of the seismic energy release, not associated with failed rifts occurs on edges of cratons (Mooney et al. 2012). An insight for the reason why IPE occur in rifts was provided by thermo-mechanical modeling by Hansen and Nielsen (2003). They demonstrated that in response to  $S_T$ , large strain accumulations are localized within rifts during their formation and reactivation. These high strain accumulations occur on discrete structures which act as local stress accumulators or concentrators. These LSCs are located in both the upper and the lower crust. IPEs occur by the release of these builtup stresses at the local stress concentrators.

### 2.4 Local rotation of the stress field

Superposition of  $S_L$  on  $S_T$  leads to its rotation locally, and the final local maximum horizontal stress,  $S_F$  is rotated by  $\gamma$  relative to  $S_T$  (Zoback 1992; Fig. 1). With

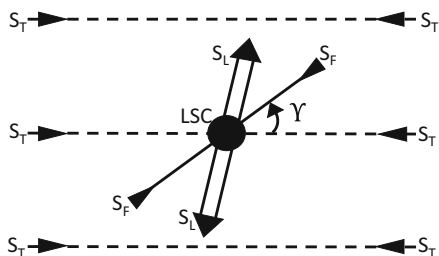


**Fig. 1** In an intraplate setting the interaction of the local stress,  $S_L$ , associated with the local stress concentrator (LSC), with the uniform regional stress field  $S_T$ , causes the final (ambient) stress,  $S_F$ , to be rotated by  $\gamma^\circ$  with respect to the regional stress field. The direction of  $S_F$  is determined by in situ measurements or by the inversion of focal mechanism data

the availability of modern seismic networks, stress field perturbations associated with LSCs, and the resulting rotations of  $S_T$  with wavelengths of tens to hundreds of kilometers are being recognized. The orientation and magnitude of the anomalous local stress buildup in a discrete volume around a LSC,  $S_L$ , depends on the kind of stress concentrator and its geometrical relationship with  $S_T$ .

For a long structure (e.g., a rift) oriented at an angle  $\theta$  to  $S_T$ , the superposition of  $S_L$ , taken to be perpendicular to the strike of the rift, causes a rotation  $\gamma$  in the direction of  $S_T$ . Sonder (1990) and Zoback (1992) showed that  $\gamma$  depends on the angle,  $\theta$  between the strike of the rift and  $S_T$ , and the ratio of the differential horizontal stress to  $S_L$ .

$$\gamma = (1/2) \tan^{-1} \frac{\text{Sin } 2\theta}{(S_{H\text{max}} - S_{h\text{min}}) / S_L - \text{Cos } 2\theta} \quad (1)$$

Thus, an increase in  $S_L$  results in an increase in  $\gamma$ . Due to uncertainties in the determination of  $\gamma$  from an inversion of focal mechanisms, only those cases for which  $\gamma \geq 15^\circ$  are considered meaningful (Zoback 1992; Mazzotti and Townend 2010). Zoback (1992) showed that in such cases,  $S_L \geq (S_{H\text{max}} - S_{h\text{min}})/2$ .

For restraining stepovers, the modeled stress buildup occurs in the vicinity of the individual intersecting faults comprising the stepover (see, e.g., Gangopadhyay et al. 2004) and as is demonstrated by a recent example (Johnson et al. 2014). For the rift pillow, the magnitude of  $S_L$  depends on the mass contrast with the surrounding volume. For intersecting faults,  $S_L$  is oriented along the direction of the shorter of the two intersecting faults and  $\gamma$  depends on the angle,  $\alpha$ , between the longer fault and  $S_T$  and the angle between the two faults ( $\beta$ ). The magnitude of  $S_L$  depends on the lengths of the two faults and the angles  $\alpha$  and  $\beta$  (Gangopadhyay and Talwani 2007). For plutons, the directions of  $S_L$  and  $\gamma$  depend on the orientation of the long axis of an elliptical pluton relative to  $S_T$ . The magnitude of  $S_L$  depends on the size of the pluton, and the ratio of its rigidity modulus to that of the surrounding volume (Campbell 1978).

### 2.5 Magnitude and areal dimensions of $S_L$

Zoback (1992) identified large-scale regional crustal features as sources of second-order stress field. Because of superposition of  $S_T$  by these regional stresses, the resultant stress field with wavelengths of hundreds to thousands of kilometers is rotated by an angle  $\gamma$

relative to the direction of  $S_T$ . In her analysis of the magnitude of various perturbing stresses, regional secondary stresses with detectable rotations of  $S_T$  (i.e.,  $\gamma > 15^\circ$ ), Zoback (1992) showed that  $S_L$  must be greater than about half the regional horizontal stress difference, i.e., approximately hundreds of megapascals. This suggests that if a detectable stress field rotation is associated with a LSC, the magnitude of associated  $S_L$  needs to be of the same order, i.e., hundreds of megapascals. Zoback et al. (1993) estimated a differential stress of  $\sim 300$  MPa at mid-crustal depths from their measurements in the KTB borehole. Mazzotti and Townend (2010) estimated the magnitudes of  $S_L$  associated with  $30^\circ$  to  $50^\circ$  rotation of  $S_T$  for the Lower St Lawrence, Charlevoix, and Central Virginia seismic zones. Assuming that the responsible seismogenic structures were oriented perpendicular to  $S_L$ , and using Eq. (1), they obtained an estimate of  $\sim 160$  to  $250$  MPa for  $S_L$  at mid-crustal depths of  $\sim 8$  km. This value was calculated on the basis of an assumed coefficient of friction of  $\mu = 0.8$  with near hydrostatic pore pressures. The estimates of  $S_L$  reduce to 20 to 40 MPa for  $\mu = 0.1$  or near lithostatic pore pressures. However, the assumptions of such anomalous parameters are not compatible with analysis by Hurd and Zoback (2012a, b), who suggest that normal values of  $\mu$  (0.6–0.8) and hydrostatic pore pressures. These values of  $S_L$  support the premise here that the stresses associated with LSCs that lead to moderate and large earthquakes are of the order of hundreds of megapascals. A larger magnitude supports our contention that in the present-day stress field, local stress perturbations associated with LSCs are the likely cause of IPE rather than the smaller regional effect of surface processes, e.g., deglaciation and erosion.

Table 1 presents a summary of examples of rotation of  $S_T$  due to a local cause. From Table 1, it is evident the areal extent of  $S_L$  associated with the LSC causing a rotation of  $S_T$  is of the order of tens to hundreds of kilometers and sometimes as small as  $\sim 20$  km.

We now examine observations complementary to those presented earlier (Talwani 2014), aimed at understanding the nature of IPEs within the framework of the unified model.

### 3 Restraining stepovers

Fault bends, intersecting faults, shallow plutons, and rift pillows have been known for a long time as locations

where stresses accumulate in response to  $S_T$ , i.e., act as LSCs (see, Talwani 2014 for a review). More recently, restraining stepovers also have been identified as LSCs (Talwani 2014). The significance of that structural style as the primary locations of larger IPEs is now being realized and will be described next.

Most strike-slip fault systems consist of numerous discrete en echelon segments and whose configuration determines their mechanical behavior. A left-stepping fault segment in a right-lateral strike-slip fault system has been variously called an anti-dilational jog, a compressional step over, stepover restraining bend, a restraining step over, and a compressive echelon fault. In a right-lateral strike-slip fault system, we will use “restraining stepover” to describe a left-stepping en echelon segment and a “releasing stepover” to describe a right-stepping fault segment. Those segments reverse and become releasing and restraining stepovers respectively in a left-lateral strike-slip fault system.

While examining the nucleation of the 1966 Parkfield and other plate boundary earthquakes, Aki (1979) suggested that fault bends and stepovers can act as stress concentrators and have a possible role in the nucleation of plate boundary earthquakes. His observation was confirmed by two-dimensional quasi-static elastic analysis of these features by Segall and Pollard (1980), which showed that restraining stepovers form potential locking points, where elastic energy can be built up and stored, and where future large earthquakes may nucleate. Sibson (1986) showed several examples of large plate boundary earthquakes that nucleated at stepovers, in agreement with Aki’s (1979) suggestion. The geometrical configuration of faults and associated seismicity near a restraining stepover described by Sibson (1986) is compatible with sand box models of restraining stepovers in strike-slip fault systems (McClay and Bonora 2001) and with the theoretical analysis by Segall and Pollard (1980).

The association of restraining stepovers (along with other LSCs) with intraplate earthquakes has been recognized at various locations (Fig. 2). The best known location of a stepover with associated IPEs is the New Madrid seismic zone (NMSZ; Fig. 2a; Russ 1982; Gomberg and Ellis 1994; Schweig and Ellis 1994; Talwani 1999; Csontos and Van Arsdale 2008). The seismicity in the NMSZ is located in and around the restraining stepover between the NE oriented Cotton Grove and North New Madrid faults. Numerical

**Table 1** Rotation of local  $S_{Hmax}$ 

Location Seismic zone	Stress Rotation Angle (° ;) (+cw)	Lateral extent (km × km)	References	
Central-Western France				
N. Armorican Massif	39	~50 to 100	Mazarbaud et al. (2005)	
S. Armorican Massif	5 <sup>a</sup>	120 × 350		
E. Massif Central	24 <sup>a</sup>	200 × 250		
Charente	17	~50 to 100		
Southeastern France				
Rhone Valley	-8 <sup>a</sup>	110 × 230	Baroux et al. (2001)	
Moyenne Durance FZ	0	70 × 210		
Digne Nappe reverse faulting domain	62	50 × 90		
Digne Nappe normal faulting domain	38 <sup>a</sup>	30 × 70		
SE of Argentera Massif	-3 <sup>a</sup>	80 × 120		
Ligurian basin	-43	50 × 200		
Eastern North America				
Lower St Lawrence	44	100 × 300	Mazzotti and Townend (2010)	
Charlevoix (Total)	32	100 × 50		
Charlevoix NW	1	20 × 40		
Charlevoix SE	47	20 × 40		
Gatineau	-5	150 × 200		
Ottawa	-8	100 × 450		
Montreal	14	100 × 150		
N. Appalachian	32	150 × 400		
C. Virginia	48	80 × 150		
E. Tennessee	-4	100 × 250		
NMSZ	6	100 × 300		
Northeastern Canada				
Hudson Bay	~ -45	~300 × 600		Steffen and Eaton (2012)
Japan				
Southwest Japan	20	35 × 250	Kawanishi et al. (2009)	
Niigata rift zone	-20	~10 × 10	Kato et al. (2006)	
Brazil				
Amazonas (rift pillow)	-75	~150 wide	Zoback and Richardson (1996)	
USA				
NMSZ (rift pillow)	10–30	~80 wide	Grana and Richardson (1996)	
India				
Kutch (rift pillow)	~50	~10 s	Mandal (2013)	
NMSZ				
Bardwell, Kentucky	40	~60	Horton et al. (2005)	
Segments near intersection of Blytheville and Reelfoot fault zones	27	~50 × 20	Johnson et al. (2014)	
Segments away from the intersection between Blytheville and Reelfoot fault zones	-3 to 5	~10 s		
NMSZ (total)	12	~200 × 100		

<sup>a</sup> Relative to direction of  $S_{Hmax}$  in local extensional stress regime

modeling has confirmed the location of seismicity with this stepover geometry (Gangopadhyay et al. 2004) and

with the locations of additional faults within the stepover (Pratt 2012).

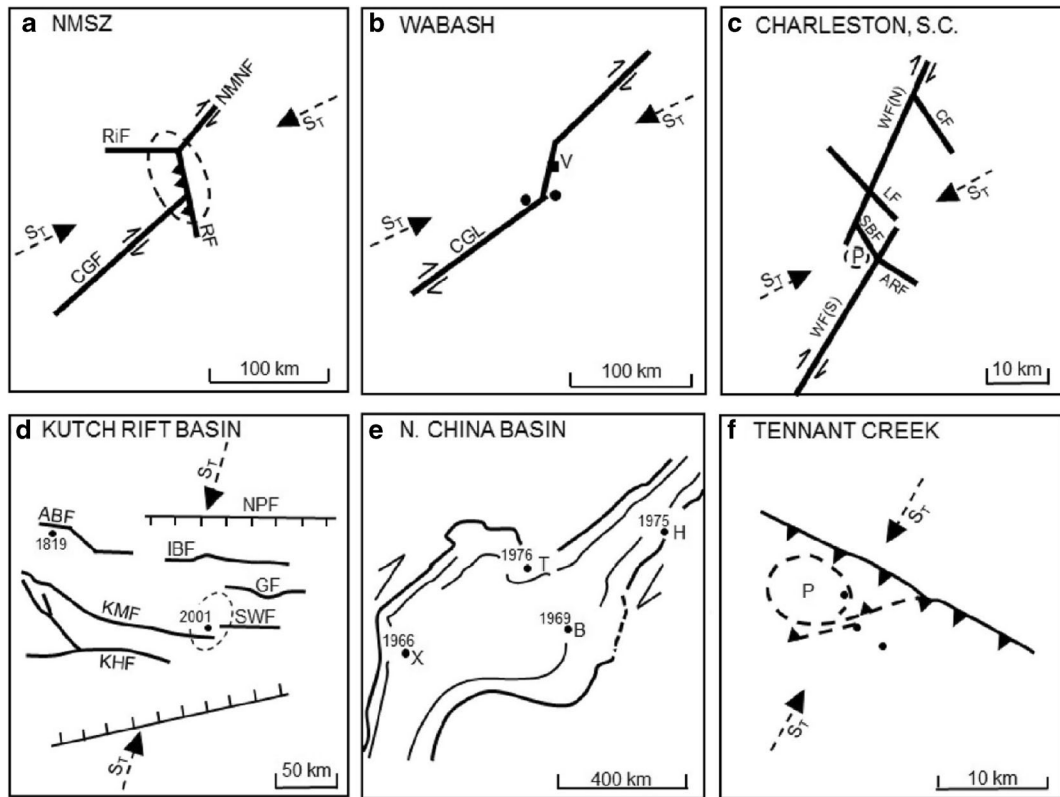


**Fig. 2** Schematic figure showing local stress concentrators in regions of major intraplate earthquakes. **a** New Madrid seismic zone lies in the region of a stepover between the NE-trending Cotton Grove and Northern New Madrid faults (CGF and NMF) and along the stepover Reelfoot fault (RF) and a buried rift pillow (dashed line), RiF denotes Risco fault. **b** Two prehistoric M >7 earthquakes (solid dots) were located in the vicinity of a restraining stepover in the Commerce geophysical lineament (CGL) near Vincennes (V) in the Wabash seismic zone. **c** The Middleton Place Summerville seismic zone near Charleston S.C. was the location of the 1886, ~M 7 earthquake in the vicinity of the restraining stepover between the northern and southern legs of the Woodstock fault (WF(N) and WF(S)) and near a buried pluton (dashed line around P). The Charleston, Lincolnville, Sawmill Branch, and Ashley River faults (CF, LF, SBF, and ARF) are also shown. **d** A series of EW faults in the Kutch rift basin were host to two major

earthquakes. The 1819 M 7.8 event occurred near the stepover in the Allah Bund fault (ABF), and the 2001 M 7.7 event in the stepover between the Kutch Mainland fault (KMF) and South Wagad fault (SWF). Other faults shown are the Nagar Parker, Island Belt, Gedi, and Katrol Hill faults (NPF, IBF, GF, and KHF). A major rift pillow was also detected below the stepover (dashed line). **e** A series of M >7 earthquakes occurred between 1966 and 1976 in the North China rift basin, a releasing stepover structure. These are the Xingtai (1966, M 7.2), Bohai (1969, M 7.4), Haicheng (1975, M 7.3), and Tangshan (1976, M 7.8). They were all associated with right-lateral strike-slip faulting on N- to NE-oriented faults. **f** Three M 6.3–6.7 earthquakes (solid dots) associated with fault scarps occurred 30 km SW of Tennant Creek, Northern Territory, were related to intersecting faults and a shallow pluton (dashed line around P).  $S_T$  shows the direction of the regional stress field

A restraining stepover in the Commerce geophysical lineament has been associated with two prehistoric M >7 earthquakes near Vincennes, Indiana in the Wabash Valley seismic zone located ~300 km to the north-northeast of NMSZ (Fig. 2b; Hildenbrand and Ravat 1997; Langenheim and Hildenbrand 1997).

Another location where the association of stepovers with IPEs has been recognized is the Middleton Place Summerville seismic zone near Charleston, South Carolina (Fig. 2c; Garner 1998; Durá-Gómez and Talwani 2009). The 1886 M ~7 Charleston earthquake

and its aftershocks were associated with the NE-trending Woodstock North and South faults and the stepover Sawmill Branch fault (Talwani and Durá-Gómez 2009).

The two largest historical earthquakes in the Kutch rift basin in western India have also been associated with stepovers (Fig. 2d; Biswas and Khattri 2003; Biswas 2005; Rastogi et al. 2014). Although detailed geological information for the area is lacking, the inferred location of the 1819  $M_w$  7.8 Allah Bund earthquake lies near a stepover in the Allah Bund fault, whose location has

been inferred from Allah Bund, the 90-km long fault escarpment associated with the surface trace of 1819 Kutch earthquake (Rajendran and Rajendran 2001; Rastogi et al. 2014; Fig. 2d). The 2001 M 7.7 Bhuj earthquake also was associated with a stepover between the Kutch Mainland and South Wagad faults. The epicenter of the Bhuj earthquake lies above a large dense mafic body located at mid-crustal depths.

Analysis of the seismicity sequence that accompanied the 1976 M 7.8 Tangshan earthquake showed that it was characterized by right-lateral slip on a series of right-stepping faults (Nábělek et al. 1987; Shedlock et al. 1987). The 1976 M 7.8 Tangshan earthquake was the last of four  $M \geq 7.0$  earthquakes within the North China rift basin in a decade. It was preceded by 1966 M 7.2 Xingtai, 1969 M 7.4 Bohai, and 1975 M 7.3 Haicheng earthquakes. Each of those earthquakes was associated with right-lateral strike-slip faulting on N- to NE-oriented faults (Nábělek et al. 1987). Activity on the releasing bends was associated with the development of the pull-apart North China rift basin (Fig. 2e; Nábělek et al. 1987). The Tangshan earthquake sequence is considered an example of the association of large intraplate earthquakes with the formation of basins. These examples also show that stress build up with both restraining and releasing stepovers can lead to IPEs.

At any location, an IPE can be associated with one or more LSC. For example, there was a sequence of three M 6.3 to 6.7 earthquakes at Tennant Creek (Australia) on 22 January 1988 (Fig. 2f). These earthquakes formed extensive fault scarps and were in response to a compressional stress field oriented  $\sim N 30^\circ E$  (Jones et al. 1991). The earthquakes occurred in response to a stress buildup on two intersecting faults expressed by the fault scarps and a shallow pluton (Bowman 1992).

Numerical modeling by Wang et al. (2013) showed that for restraining stepovers, smaller fault spacing (or separation proportional to fault overlap) leads to an increase in “the maximum value of the sum of large shear drops,” i.e., larger magnitude events. However, there is no consistent relationship for releasing stepovers.

#### 4 Observation of anomalous pockets local stress rotation

With the availability of modern seismic networks detailed focal mechanism data can be inverted to obtain  $S_F$ . Increasingly local stress field perturbations associated with

LSCs and the resulting rotations of  $S_T$  with wavelengths of tens to hundreds of kilometers are being recognized. The orientation and magnitude of  $S_L$  in a discrete volume around a LSC, depends on the kind of stress concentrator and its geometrical relationship with  $S_T$  (Talwani 2014).

Talwani (2014) presented examples of local rotations of  $S_T$ . Table 1, taken from that study with an additional recent example, lists instances where such a rotation has been observed. Due to limitations in the quality of data, and inversion techniques used to obtain the directions, only those cases with  $\gamma \geq 15^\circ$  are considered meaningful as examples of local stress rotation (Mazzotti and Townend 2010).

Co-seismic stress rotation on adjacent faults has often been observed following large earthquakes. That however, is not the case for the earthquakes listed in Table 1. Instead, I interpret them to be a result of a temporal growth of  $S_L$ , such that earthquakes occur when the magnitude of  $S_L$  approaches that of  $S_T$ . Table 1 lists examples of local stress rotation, and the approximate areas over which they are observed in intraplate settings in France, Eastern North America, northeastern Canada, Japan, Brazil, and India. The quality of seismicity data and geologic information for each example vary considerably from one location to another, and details about each entry can be found in Talwani (2014). Among those examples are two with excellent correlative geological and seismological observations, where the direction of  $S_F$  in small neighboring clusters of seismicity differ by more than  $20^\circ$ . Analyses of these two examples within the framework of the unified model provide further insight into the nature of IPEs.

##### 4.1 Anomalous stress rotation near Charlevoix in the St Lawrence fault zone

Mazzotti and Townend (2010) inverted focal mechanisms to determine the local state of stress in ten seismic zones in central and eastern North America. Those authors compared the azimuth of the seismically determined stress field,  $S_F$  in our nomenclature, with  $S_T$  obtained from relatively shallow boreholes within 250 km of the seismic zones. For four seismic zones, the two azimuths were essentially parallel. However, a statistically significant clockwise rotation of  $\sim 30\text{--}50^\circ$  was found for Charlevoix, Lower St Lawrence, and Central Virginia seismic zones and to a lesser extent for North Appalachian seismic zone.

For the entire Charlevoix seismic zone, a clockwise rotation of  $32^\circ$  relative to  $S_T$ , was obtained from borehole

data. With the availability of a larger amount of seismicity data Mazzotti and Townend (2010) were able to determine the direction of  $S_F$  for each of the two NE-SW trending parallel clusters of seismicity located ~15 km apart (Fig. 3a). A significant difference in the directions of  $S_F$  directions was observed for the two clusters.

For the NW cluster lying along the border faults of the St. Lawrence Rift System (SLRS), oriented N 40° E, the median azimuth of  $S_F$  is N 55° E, essentially along the direction of  $S_T$ , N 54° E (Fig. 3a). For the SE cluster, separated from the NW cluster by a 5–10-km aseismic zone associated with a high velocity body, the median

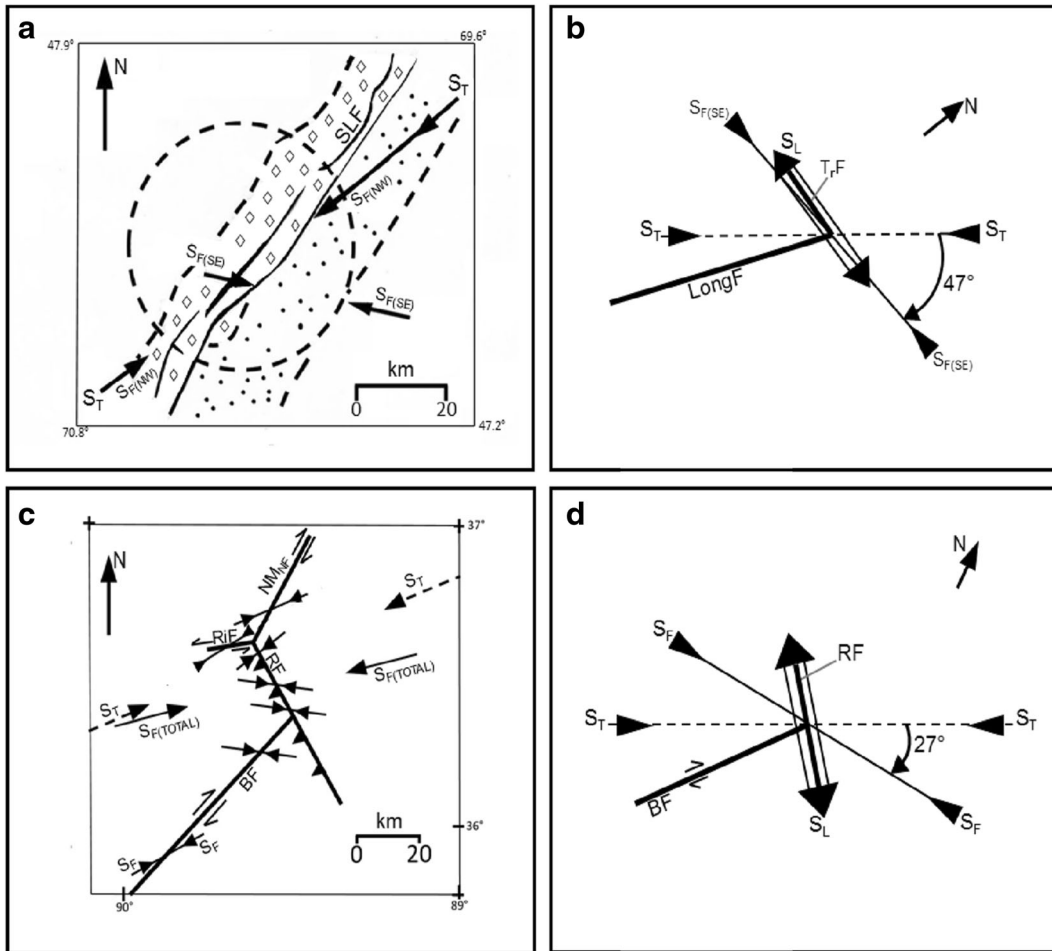


**Fig. 3** a Dashed and solid NE-trending lines are the faults of the Saint Lawrence rift basin. In the Charlevoix area, the most prominent of these is the St. Laurent fault (SLF). The dashed circular line shows the outline of the impact crater. The shaded area represents the NW cluster of seismicity, with  $S_{F(NW)}$ -oriented N 55° E, essentially along  $S_T$ , oriented N 54° E. For the SE cluster of seismicity (dotted pattern),  $S_{F(SE)}$  is oriented N 101° E, rotated 47° relative to  $S_T$ . Fault lines and stress directions are from Mazzotti and Townend, (2010). b Schematic figure showing the local stress  $S_L$  (arrow with double lines) associated with the LSC (the intersection of the longitudinal and transverse faults (solid lines, LongF and TrF)). Interaction of  $S_L$  (lying along TrF, oriented 300°), with the regional stress,  $S_T$  (oriented 54°) causes the final stress,  $S_F$  to be rotated along 101°, i.e., with a clockwise rotation of 47° relative to  $S_T$ . c Faults and local stress directions in the New Madrid seismic

zone from Johnson et al.(2014). The local stress directions  $S_F$  (converging arrows around faults, solid lines) have been derived for seven segments.  $S_F$  is oriented 70° for the southwestern part of Blytheville fault (BF), the northern part of the Reelfoot fault (RF), the North new Madrid fault (NNMF), and 65° for the Risco fault (RiF).  $S_F$  is oriented 97° for the northeastern part of BF, and the central and southern parts of the RF, showing a 27° clockwise rotation with respect to  $S_T$  oriented at 70° (dashed arrows). The ambient stress direction for the whole NMSZ,  $S_{F(TOTAL)}$  is oriented 79°. d Schematic figure showing the local stress  $S_L$  (arrow with double lines) associated with the LSC (the intersection of BF and RF, solid lines). Interaction of  $S_L$  (lying along RF, oriented 338°), with the regional stress,  $S_T$  (oriented 70°) causes the final stress,  $S_F$  to be rotated along 97°, i.e., with a clockwise rotation of 27° relative to  $S_T$

direction of  $S_F$  is along N 101° E, i.e., with a clockwise rotation of 47° relative to  $S_T$  (Fig. 3a).

Exploring the effect of the Devonian age impact crater on the seismicity of the Charlevoix seismic zone, Baird et al. (2010) noted that most of the larger events were located outside the crater, while increased lower magnitude seismicity occurred within it. The result of their 3-D stress analysis of the interaction of the rift and crater faults, suggested that there was a rotation of  $S_T$  on the periphery of the crater. In their model, lacking structural complexity, they assumed longitudinal (parallel to the rift) faults, and no transverse faults, within a homogeneous background. Predictably, a stress build up was observed along the longitudinal faults, but only with the assumption that they were very weak, i.e., with very low coefficient of friction and/or with high pore pressures. As we have seen earlier (Sect. 2.5) Hurd and Zoback (2012a, b) show that such anomalous weak faults are not needed to explain the observed seismicity in Eastern Canada. This suggests that the modeling results with their simplified assumptions are not conclusive, and the cause of the observed stress rotation may lie elsewhere.

Mazzotti and Townend (2010) however found that the rotation of  $S_T$  was not limited to the periphery of the crater but was also observed to its NE. The unified model provides a possible explanation for the difference in directions of  $S_F$  in the NW and SE clusters of the Charlevoix seismic zone, based on geological and geophysical field observations.

Geological and geophysical mapping by Tremblay et al. (2003) revealed the presence of two sets of fault trends with mutual crosscutting relationships in the Charlevoix area of the St. Lawrence rift system. The conjugate structures were interpreted to be a result of the same tectonic event. Onshore, the longer longitudinal faults of SLRS are oriented along N 25° E, N 40° E, and N 70° E, with the N 40° E-oriented St Laurent fault (SLF) the most prominent fault (Fig. 3a). The shorter (<10 km long) transverse faults are bounded by the longitudinal faults. Tremblay et al. (2003) suggest that the longitudinal faults of the SLRS are result of the development of an echelon faults trending parallel to the rift axis, and transverse structures, oriented N 290° E and N 310° E (Tr.F in Fig. 3b), represent transfer faults. The observation of striated or slicken lined fault planes on the two sets of faults were interpreted as evidence of normal-sense movements on the longitudinal faults and strike-slip faulting on the transverse faults.

Seismic profiles in the St. Lawrence River revealed submarine structures coincident with SLF and other structures similar to those onshore, suggesting that the pattern of NE-SW longitudinal rift faults and shorter NW-SE trending transfer faults mapped onshore continues under the St. Lawrence River (Tremblay et al. 2003).

According to a parametric study (Gangopadhyay and Talwani 2007), favorably oriented intersecting faults (optimally, with the main fault at  $\sim 45 \pm 15^\circ$  to  $S_T$ , and the shorter intersecting fault at  $90 \pm 30^\circ$  to the main fault), act as LSCs, with  $S_L$  oriented along the shorter fault (Talwani 2014). For faults oriented along  $S_T$ , or at a small angle to it, both  $S_L$  and  $S_F$  will be along  $S_T$ . Applying the results of the parametric study suggests that the seismicity in the NW cluster is associated with the longitudinal faults, and  $S_F$  is also oriented along  $S_T$  (Fig. 3a). In the case of the transfer faults, the fault intersections acts as LSCs and the local stress accumulations,  $S_L$  occurs along them (N 120° ± 10° E) and interacts with  $S_T$  (oriented N 54° E) such that the final resulting stress  $S_F$ , inferred from the seismicity data is along N 101° E, or rotated clockwise by 47° relative to  $S_T$  (Fig. 3b). Thus, the difference in the azimuth of  $S_F$  in the NW and SE clusters of the Charlevoix seismic zone can be explained by the nature and geometry of the LSCs associated with them, with a plausible contribution from the modification of the local stress field by the interaction of the regional faults with those due to the crater.

#### 4.2 Anomalous stress rotation in New Madrid seismic zone

Johnson et al. (2014) inverted focal mechanism data for 309 earthquakes in the NMSZ with a magnitude range from  $\sim 1$  to 4.6 to obtain the direction of the local maximum horizontal stress,  $S_F$ . For the entire set, the direction of  $S_F$ , N 79° E ± 30°, was rotated  $\sim 9^\circ$  with respect to (their estimate of) the direction of the regional maximum horizontal stress,  $S_T$ , (ENE),  $\sim$ N 70°. The inferred direction of  $S_F$  for NMSZ was in general agreement with earlier studies: 82° (Mazzotti and Townend 2010) and 79° (Hurd and Zoback 2012b).

Johnson et al. (2014) also determined the direction of  $S_F$  associated with seven fault segments comprising the NMSZ—the northeastern and southwestern parts of the

NE-striking “southwestern segment” comprising the Blytheville fault zone (BF; also referred to as the Cotton Grove fault or the Axial fault) and the Blytheville arch; a NW-trending central segment (Reelfoot fault (RF)), which was further sub-divided into its northern, mid- and southern parts, a northeastern segment along the New Madrid North fault, and a northwestern segment along the Risco fault. They found the orientations of  $S_F$  for the mid- and southern sections of Reelfoot fault, and along the upper part of the southwestern segment, all to be N 97° E. All three of these sections are within 50 km of the intersection between Blytheville and Reelfoot faults (Fig. 3c). This direction of  $S_F$  is rotated 27° clockwise with respect to  $S_T$  (Fig. 3d).  $S_F$  is N 70° E for each of the lower part of the southwestern segment, the northern part of RF, and NNMF, and N 62° E for Risco fault, i.e., along or within of 10° of  $S_T$  (Fig. 3d).

The unified model can explain the observed 27° clockwise rotation in the direction of  $S_F$  in the New Madrid seismic zone (Johnson et al. 2014). This rotation was observed in a  $\sim 50 \times 20$ -km area in the vicinity of the intersection between the NE-striking Blytheville fault zone and the NW striking Reelfoot fault (Table 1). This fault intersection is interpreted to act as a local stress concentrator (Gangopadhyay and Talwani 2007). It also lies atop a buried rift pillow, a LSC, for which Grana and Richardson (1996) estimated a clockwise rotation of 10° to 30° of  $S_F$ , relative to  $S_T$ . The observation of Johnson et al. (2014), a clockwise rotation of  $S_T$  by 27° is in sync with the expectations of the unified model (Figs. 1 and 3d).  $S_L$  due to the LSC lies along RF and interacts with  $S_T$  such that  $S_F$  is rotated 27° relative to  $S_T$  (Fig. 3d).

The orientation of the Reelfoot fault is almost orthogonal to  $S_T$  and not optimal for stress rotation. Consequently away from Blytheville fault, along the Reelfoot fault,  $S_F$  is along  $S_T$  ( $\pm 10^\circ$ ; Fig. 3c).

These two examples of large differences in the direction of  $S_F$  in neighboring regions of seismicity (47° between the NW and SE clusters in the Charlevoix seismic zone, located 15 km apart), and 27° between the seismicity near the intersection of the Blythewood and Reelfoot faults, and in neighboring regions, located tens of kilometers away within the NMSZ) are interpreted to be because of differences in the directions of  $S_L$  at the LSCs, and, resultantly in the directions of  $S_F$  at these locations.

## 5 Roaming or non-repeat earthquakes

The occurrence pattern of IPEs is much less regular in both space and time as compared with their plate boundary counterparts. Large earthquakes are much less frequent and more widespread in continental intraplate regions, as compared with those at plate boundaries. Differences in the seismogenesis of IPEs with respect to their plate boundary counterparts can be gleaned by comparing the spatial and temporal pattern of their occurrence. The spatio-temporal patterns of IPEs also vary considerably from one region to another. This pattern can be observed in the historical accounts and inferred from paleo-seismological data, as shown by the following examples.

The 2000-year-long record for the intraplate North China Block (NCB) was analyzed by Liu et al. (2011, 2014) for the spatial and temporal pattern of historical events. In this  $\sim 1000 \times 1000$  km region, those authors found that more than 100 large ( $M > 6.0$ ) earthquakes have occurred since 23 BCE. They found “long distance roaming” of events between widespread fault systems, i.e., no  $M > 7$  “repeat earthquake” had ruptured the same fault segment twice in the studied historical period. While many of these large earthquakes migrated between the Shanxi and Wiehe rifts, and between those rifts and the North China Plain, they did find evidence of episodic large earthquakes separated by thousands of years of quiescence on the same fault segment.

In this time period, there were periods of intense activity, e.g., in the decade following 1966. Five earthquake sequences, Xingtai (five events with  $M > 6.0$  in 1966), Hejian ( $M_s$  6.3, 1967), Bohai ( $M_s$  7.4, 1969), Haicheng ( $M_s$  7.3, 1975), and Tangshan ( $M_s$  7.8, 1976) occurred sequentially from southwest to northeast, within  $\sim 2 \times 10^5$  km<sup>2</sup>, Cenozoic age North China (rift) basin (Shedlock et al. 1987; Wang et al. 1997). This region has been quiet since that activity. Scholz (1977) suggested that the northeasterly progression of earthquakes could have been associated with a “deformation front.” However, the nature of this front was not specified.

The historical pattern of seismicity in the past two centuries also suggests the occurrence of at least four large ( $M > 6$ ) non-repeat earthquakes in the  $\sim 270 \times 150$  km Kutch rift basin in western India. Plus, there is evidence of at least another large older event from archeological data (Fig. 4). The four large earthquakes are the 1819  $M$  7.8 earthquake on the Allah Bund fault; the 1845  $M$  6.3 earthquake on the Kutch Mainland

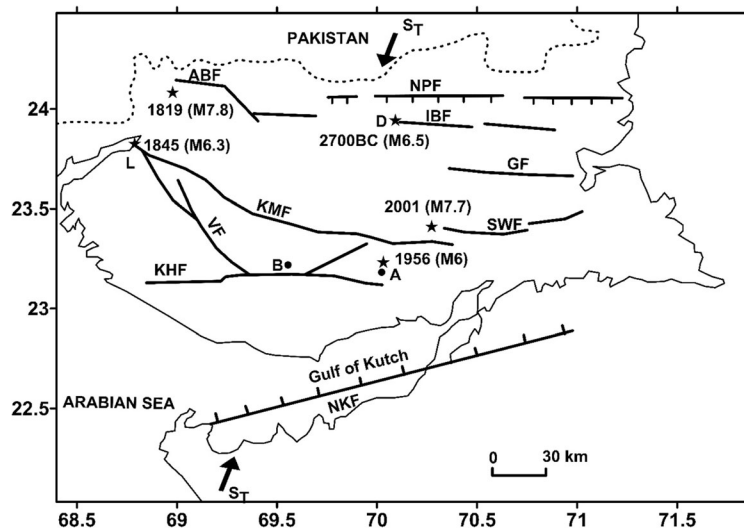


**Fig. 4** The Kutch rift basin lies between Nagar Parker (*NPF*) and North Kathiawar faults (*NKF*). Historical earthquakes in 1819, 1845, and 2700 BC are inferred to be associated with the Allah Bund (*ABF*), Kutch Mainland (*KMF*), and Island Belt faults (*IBF*), respectively. Instrumentally located 1956 Anjar (*A*) and 2001 Bhuj

(*B*) earthquakes were associated with the Katrol Hill (*KHF*; ?) and South Wagad faults (*SWF*), respectively. *D* and *L* show the locations of old historical towns at Dholavira and Lakhpat.  $S_T$  shows the direction of the regional  $S_{Hmax}$ . (fault map courtesy B.K. Rastogi)

fault, which destroyed Lakhpat and the 1956 Anjar earthquake on the Katrol Hill (?) fault and the widely destructive 2001 M 7.7 Bhuj earthquake on the stepover near South Wagad fault (Rastogi et al. 2014). On the basis of paleo-archeological investigations and historical reports, Bisht (2011) suggested that in ~2700 BCE, an estimated M 6.5 earthquake destroyed Dholavira on the Island Belt fault (Fig. 4).

This pattern of non-repeat earthquakes in an intraplate setting has also been observed on a smaller scale. Closely monitored reservoir-induced earthquakes offer an excellent opportunity to study the spatio-temporal pattern of earthquake nucleation in a controlled setting in an intraplate region, even though the seismicity is primarily associated with pore pressure changes. Since 1962, reservoir-induced seismicity with thousands of earthquakes, including a M 6.3 event in 1967, has been continuously observed in the ~30×20-km area in the vicinity of the Koyna and Warna reservoirs in western India. Nineteen larger ( $M \geq 5.0$ ) events that occurred between 1967 and 2003, associated with water-level fluctuations in the two reservoirs, and located with an accuracy of better than about a kilometer, reveal an interesting spatio-temporal pattern (Fig. 5). None of the earthquakes occurred at a location occupied by an earlier  $M \geq 5$  event (numbered circles in Fig. 5; Talwani and Durá-Gómez 2009).

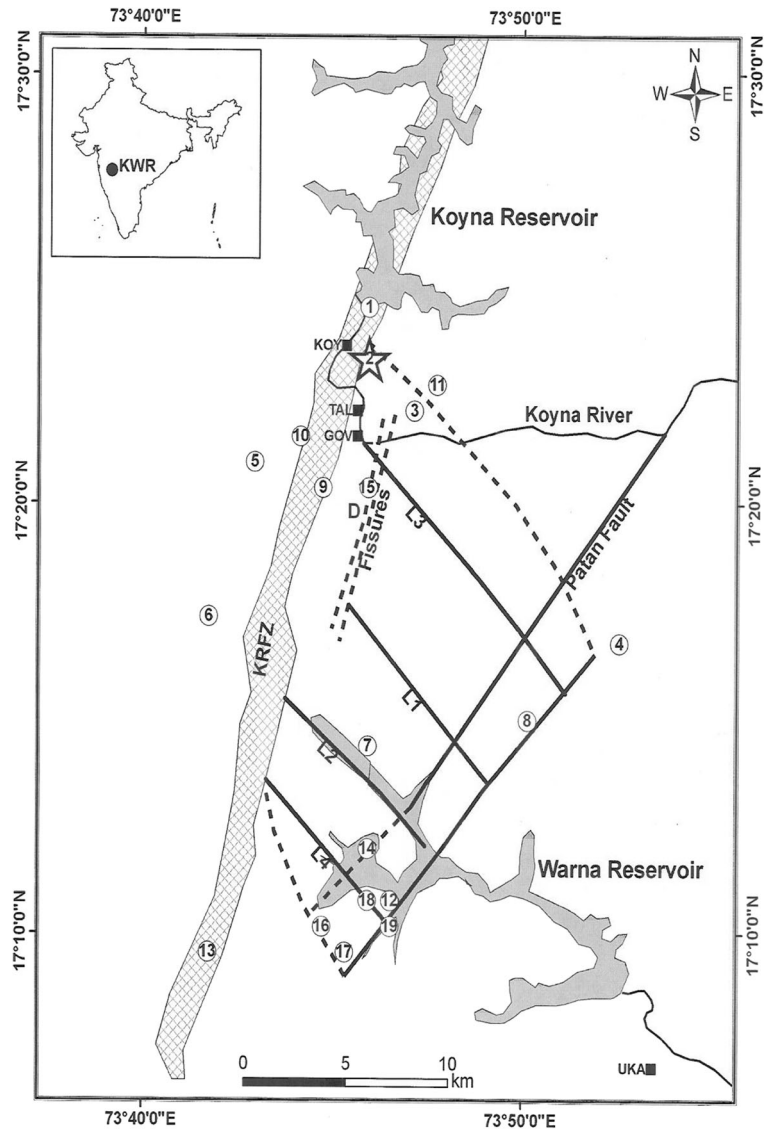
At a yet smaller scale, low-level ( $M < 3$ ) reservoir-induced seismicity was observed at Lake Jocassee in northwestern South Carolina in the mid-1970s. After the initial M 3.2 event in November 1975, 12 M 2–3 aftershocks occurred in a 10×8 km region in the vicinity of the Lake Jocassee dam. None of these events or their aftershocks, located with a hypocentral accuracy of better than 0.5 km, occurred in the same location as an earlier  $M > 2$  event (Talwani 1981).

Summarizing, the spatio-temporal pattern of seismicity in these examples reveals an interesting pattern (Table 2). The observation periods and the study areas vary greatly. However, a common feature is that in none of the cases was there a repeat earthquake at the location of the main event during the period of study. In each case, the main event did not occur at a location occupied by a previous main event in the study period. These observations suggest that non-repeat earthquakes may be a characteristic feature of IPEs.

### 5.1 Paleo-seismological investigations

Most intraplate regions lack such detailed historical or instrumental information, and the spatio-temporal pattern of prehistoric seismicity has to be inferred from paleo-seismological data. The results of paleo-seismological investigations, however, are limited due to uncertainties in the inferred dates and locations of the

**Fig. 5** Tectonic framework and location of  $M \geq 5.0$  reservoir-induced events in the Koyna Warna region in western India, 1967–2003. (From Durá-Gómez and Talwani 2010)



prehistoric events. Also at any location, a “sequence” of large earthquakes can last from a few minutes (Charleston, 1886), a few days (Xingtai, 1966), to a few months (New Madrid, 1811–1812). Usually, the

paleo-seismological data are incapable of resolving individual events, and the sequence is inferred as one “event” from the paleo-seismological data. Although the earthquakes interpreted from paleo-seismological

**Table 2** Examples of non-repeat earthquakes

Location	Area (km × km)	$M_{MAX}$ of non-repeat Eqs.	Observation period (year).	Reference
East China Basin	1000 × 1000	$\geq 7$	2000	Liu et al. (2014)
Kutch Rift Basin	270 × 150	$\geq 6$	~200	Talwani (2014)
Koyna-Warna Region (RIS)	30 × 30	$\geq 5$	~50	Durá-Gómez and Talwani (2010)
Lake Jocassee (RIS)	10 × 8	$\geq 2$	~4	Talwani (1981)

data lack both an exact date and location, they do identify episodes of large earthquakes separated in time by thousands of years. Currently, there are three intraplate regions where detailed paleo-seismological data are available.

In the New Madrid seismic zone, paleo-seismologic investigations have revealed the occurrence of five earthquake sequences, including 1811–1812, which have occurred within the last 4300 years (CE 1811–1812,  $1450 \pm 150$ ,  $900 \pm 100$ ,  $300 \pm 200$ , and 2350 BCE  $\pm 200$  years) (Tuttle et al. 2002, 2005). Paleoliquefaction data also suggest that like the 1811–1812 earthquakes, those in CE 1450, 900, and 2350 BCE were also associated with multiple events within a short period (Tuttle et al. 2002, 2005).

Paleo-liquefaction data are usually inadequate in identifying the exact location of the seismic source associated with a particular liquefaction feature mapped on the ground surface. However, in calculations of the recurrence rates of similar events, it has been tacitly assumed that all these prehistoric events were associated with one seismic source. This assumption may not be valid as it ignores the presence of other LSCs (potential seismogenic structures) which are currently inactive, which could have been associated with the prehistoric events. Clearly, there is need for caution in assigning seismic sources within the  $\sim 200 \times 100$ -km NMSZ.

In addition to the temporal clustering in the NMSZ, within the Reelfoot rift there is paleo-seismological evidence of two large earthquakes. These occurred  $\sim 6100$  years BP in the Wabash Valley (Munson et al. 1997) and  $\sim 5500$  years BP in eastern Arkansas (Al-Shukri et al. 2005), located  $\sim 400$  and  $\sim 300$  km NE and SW, respectively, of the NMSZ.

Paleo-seismological studies in the South Carolina Coastal Plain, the location of the historic 1886 Charleston earthquake, revealed the occurrence of abundant sand blows associated with prehistoric earthquakes. Dating of 121 sand blows revealed the occurrence of seven large earthquakes within the past 6000 years, capable of generating sand blows at distances up to 100+ km (Talwani and Schaeffer 2001). The source of each paleo-earthquake was inferred from the distribution of contemporary sand blows. The distribution of sand blows underscored the importance of the local site conditions associated with the generation of the sand blow (soil profile, depths to, and thickness of, the source sands and water table). For example, in a drainage ditch at Sampit, with favorable site conditions, there was

evidence of paleo-earthquakes  $\sim 500$ , 1000, and 1600 YBP. Contemporary sand blows of the two latest paleo-earthquakes were found  $\sim 200$  km away, while those for the 1600 YBP event were mostly within 50 km and at one location  $\sim 100$  km away. Epicentral locations were inferred to be near Charleston for the 500 YBP and 1000 YBP events and near Sampit for the 1600 YBP event. These observations demonstrate the difficulty in the accurate determination of the location of the source of prehistoric earthquakes, an important element in seismic hazard estimation, from the location of sand blows.

Due to a short historical, and shorter instrumental record of seismicity in Australia, the data are inadequate to accurately identify and outline the buried seismogenic features and assess their seismogenic potential. Clark et al. (2014) solve the problem of a short historical and poorly constrained seismicity record by using a geological record of well-preserved fault scarps. Evaluation of more than 300 fault scarps and other geomorphic features dating back to more than 10 Ma preserved in the geological record, led Clark et al. (2014) to conclude that contrary to the historical record, the paleo-record, which essentially captured events of  $M > 5.5$ , suggested a pattern of temporal and spatial clustering of earthquakes, which is apparent at the scale of a single fault, and at a regional scale. They found temporal clustering of events over a period of a few thousand years, separated by periods of quiescence lasting hundreds of thousands years. This is in contrast with an inferred average recurrence time of about 500 years in the NMSZ and the South Carolina Coastal Plain for earthquakes occurring in recent Holocene.

These examples of the spatial and temporal pattern of IPEs, occurring on different LSCs spread over large regions, and over thousands of years, differ markedly from their plate boundary counterparts, where repeat earthquakes occur over the same, well-defined faults, with shorter (approximately hundreds of years) repeat times, suggesting the need for caution when applying methods of seismic hazard analysis developed for plate boundary earthquakes.

## 6 Observations from Kutch, western India

The Mesozoic-age Kutch Rift Basin (KRB) in western India is among the most active intraplate regions in the world and has been the location of intensive geological and geophysical investigations since the early 1970s and

seismicity studies with the deployment of seismic network since 1976. Although sporadic geodetic investigations have been carried out before 2001, they were of poor quality (Wallace et al. 2006). The 2001 M 7.7 Bhuj earthquake that occurred in KRB was followed over the next 12 years by multidisciplinary studies carried out with fine resolution and coverage. This rich data base, a rarity in an intraplate setting provided a unique opportunity to study the seismogenesis of IPEs. These studies consisted of seismicity monitoring on an extensive Gujarat statewide seismic network of 76 broadband seismographs including 40 in the  $270 \times 150$  km KRB; ground motion monitoring with a 22 station GPS network, three sets of InSAR data, active fault investigations and subsurface mapping with various geophysical techniques (Rastogi et al. 2014).

The results of those investigations have been used to study the seismogenesis of the observed intraplate seismicity (Rastogi et al. 2014). The main elements of these investigations, as described by Rastogi et al. (2014), are crustal structure, seismicity, ground movement, and seismogenesis. A summary of their findings is presented below and examined within the framework of the unified model.

**Crustal structure** Subjecting the KRB to north–south compression promotes reverse faulting on the east–west faults and strike-slip motion on the transfer faults. As a result, the east–west KRB consists primarily of six sub-parallel east–west striking moderately dipping faults which bound three uplifts, and a few NW-SE and NE-SW striking transfer faults (Fig. 4), some of which extend to large depths, dividing the region into discernible blocks. KRB was found to have a thin crust overlying a thinned lithosphere. Seismic tomography led to the detection of a  $\sim 60$ -km-long (NS) and  $\sim 40$ -km-wide (EW),  $\sim 15$ - to  $20$ -km-thick solid mafic body lying at a depth of  $\sim 10$  km within embedded low seismic velocity zones interpreted to be related to fractures containing of meteoric fluids. Rastogi et al. (2014) interpret the high-density mafic body to act as a local stress concentrator associated with the Bhuj earthquake, which nucleated at mid-crustal depths.

**Seismicity** Following the 26 January 2001 M7.7 Bhuj earthquake with an estimated depths of 16 km (USGS) and 22–23 km (ISC), aftershocks through 2003 (including 15 with  $M \geq 5.0$ ) were concentrated in the  $40 \times 40$ -km rupture area. Between 2006 and 2012, there was an

outward progression of seismicity to both North and South, with the most distant event 240 km away. The authors speculated that this delayed outward migration of seismicity was associated with a stress pulse triggered by a 22-MPa stress drop associated with the 2001 earthquake. This stress pulse was associated with M 5 events on distant faults in both directions (see, Rastogi et al. 2014 for details).

**Ground movement** Biannual campaign-mode GPS observations between 2001 and 2006 were followed by continuous observations on a 22 permanent station network since 2006. The results showed that co-seismic horizontal strain rates of 12 mm/year (in the first half of 2001) decayed to a background level of  $2\text{--}5 \pm 1$  mm/year by the end of 2003. However, evidence of continuous large vertical strain rates of  $2\text{--}13 \pm 3$  mm/year were observed at discrete stations located near the epicenter of the Bhuj earthquake and up to 75 km away from it. These isolated pockets of large vertical strain rates were confirmed by interferograms generated from European and Japanese satellite data.

**Seismogenesis** Rastogi et al. (2014) recognized the seismicity being due to inversion related deformation within KRB in response to NS compression associated with plate tectonic forces. The anomalous large, buried mafic body (rift pillow?), and the overlying constraining stepover were identified as potential local stress concentrators associated with the 2001 earthquake.

We will examine these data within the framework of the unified model, especially concentrating our examination on the isolated pockets of elevated vertical strains being indicative of potential LSCs with associated seismicity.

## 6.1 Comparison of seismicity and geodetic data

The large co-seismic horizontal strain rates observed in the first 6 months after the Bhuj earthquake, decayed rapidly in the following 2 years. However, even after 2007, large vertical strain rates continued to be observed at four locations on the GPS data. To confirm their actuality, an independent set of measurements were obtained and compared with the contemporary seismicity.

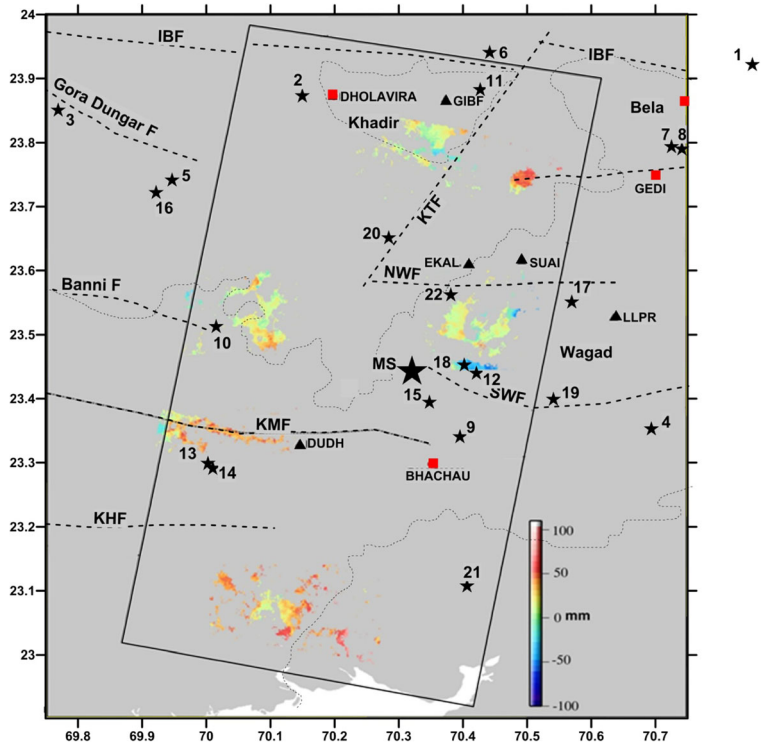
Interferometric Synthetic Aperture Radar (InSAR) studies begun in 2008 complemented earlier GPS

studies (Rastogi et al. 2012, 2014). Using the European Space Agency's Environment Satellite (ENVISAT), and its advanced synthetic aperture radar (ASAR) from June 2008 to October 2009, the interferogram generated with Differential Interferometric Synthetic Aperture Radar (DInSAR) showed evidence of vertical deformation rates from 7 to 27 mm/year at distinct locations within 75 km of the epicenter of the 2001 main shock (Fig. 6; Rastogi et al. 2012). These anomalous vertical movement rates were found to be located in the vicinity of the south-dipping Katrol Hill, Kutch Mainland, Gedi, and Island Belt faults (KHF, KMF, GF, and IBF; in Fig. 6). An anomalous pocket of high subsidence rate ( $\sim 20$  mm/year) was observed in the Wagad uplift to the north of the SWF. Another pocket of high vertical uplift was located on the Wagad uplift enclosed by the south dipping North Wagad (NWF) and the north dipping South Wagad faults, and to its west near the Banni fault. Additional ENVISAT ASAR data from 2004 to 2007 and the Japanese Aerospace Exploration Agency's Advanced Land Observing satellite (ALOS), with its Phased Array type L-band Synthetic Aperture Radar (PALSAR) data from 2007 to 2010 confirmed the magnitude and locations of the anomalous high vertical rates

of deformation (Rastogi et al. 2014). (These are the only InSAR data that were collected for the study area).

These InSAR data complemented earlier campaign-mode post-seismic (2001 earthquake) GPS data (2001–2005; Reddy and Patil 2008) and data acquired after from a network of 22 continuously recording and 11 campaign—mode GPS stations (Rastogi et al. 2014). The results of the GPS data (Rastogi et al. 2012, 2014) showed that the initial co-seismic horizontal deformation rate of  $\sim 12$  mm/year had reduced to a background level of  $2\text{--}5 \pm 1$  mm/year by 2003. However, a large vertical deformation rate (5 to 13 mm/year) was detected at four GPS sites, Dudhar (DUDH near KMF,  $10 \pm 3$  mm/year); Gadaha (GIBF near IBF,  $13 \pm 3$  mm/year); Lilpur (LLPR in the Wagad uplift,  $6 \pm 3$  mm/year); and Fahegarh (on the Gedi fault,  $5 \pm 3$  mm/year). The locations of these stations, taken from Rastogi et al. (2014) are shown in Fig. 6. These data were confirmed by the high vertical deformation rates obtained from InSAR data, i.e., long after the co-seismic horizontal strain was reduced to original background levels, there are pockets of high vertical deformation in the epicentral area of the Bhuj earthquake. To examine if these isolated pockets of high strain were evidence of the presence of

**Fig. 6** Differential interferogram showing range changes in line of sight generated from ENVISAT advanced synthetic aperture radar between June 2008 and October 2009 in the region surrounding the M 7.7 Bhuj earthquake (*large star*). Large uplifts were observed in the vicinity of faults. *Triangles* show location of GPS stations. Locations of vertical deformations (*color*) are compared with  $M \geq 4.0$  aftershocks (*numbered stars* correspond to Table 3). The InSAR interferogram courtesy Dr. Sreejith of the Indian Space Research Organization, Ahmedabad, India. Figure courtesy Dr. BK Rastogi



local stress concentrators, their locations were compared with seismicity data.

Following the 2001 Bhuj earthquake, through 2012, there were 22 earthquakes with  $M \geq 4.0$  in the epicentral area (Table 3). The locations of these numbered earthquakes in Table 3 are compared with the locations of the anomalous deformation rates obtained from InSAR and GPS data in Fig. 6. We note that of these 22 events, only 12 occurred inside the area covered by InSAR (large rectangle). Six of these occurred in areas showing anomalous vertical deformation—nos. 13 and 14 near the Kutch Mainland fault, no. 10 near the Banni fault, and nos. 12, 18, and 22 in the Wagad uplift (Fig. 6). Event no. 17 was located within the Wagad uplift, outside the InSAR survey area, but the nearby GPS station LLPR showed elevated rates of vertical deformation. Three events occurred in the vicinity of pockets of anomalous vertical deformation near

Khadir Island (nos. 2 and 11, possibly associated with the Island Belt fault, and no. 20 associated with the Khadir Transfer fault). Events nos. 9 and 15 occurred in the stepover zone between KMF and SWF, the location of the mainshock. Event no. 21 occurred in an area with no exposed fault.

The occurrence of seven events in regions of vertical deformation suggests that they may have been associated with a buildup of stresses at those locations. We interpret the structures where these stresses are built up to be LSCs.

This interpretation suggests that with focused geodetic observations using InSAR and a dense network of GPS stations, it may be possible to detect buildup of stresses at different LSCs. These geodetic data also explain that while geodetic strains may be elevated in local pockets in the vicinity of the LSCs, they are negligible away from them, resulting in observed low average strains rates over large areas.

**Table 3**  $M \geq 4$  events in KRB following the 2001 Kutch earthquake

SN	Y	M	D	Lat	Long	Dep. km	Mag $M_w$	Mag USGS	Location	Mechanism
	2001	1	26	23.44	70.31	16.0	7.7	7.7	18 km NW of Bhachau North Wagad F.	Thrust
1	2004	1	8	23.91	70.90	20.0	4.2		Gedi/Is. Belt F.	
2	2004	6	7	23.87	70.15	29.4	4.2		Dholavira/Is. Belt F.	
3	2005	3	8	23.85	69.74	11.6	4.3		Gora Dungar F.	
4	2005	10	8	23.35	70.69	24.0	4.5		South Wagad F.	
5	2005	10	9	23.74	69.93	6.6	4.3		Gora Dungar F.	
6	2006	2	03	23.92	70.44	28.0	5.0	4.5	Gedi F., foreshock	Thrust
7	2006	3	07	23.79	70.73	3.0	5.6	5.5	Tr. Bela F./Gedi F., ms	left lateral
8	2006	4	06	23.78	70.74	3.0	4.8	5.0	Gedi F., aftershock	Thrust
9	2006	4	06	23.34	70.39	29	5.6	5.5	Lakadia, SWF	
10	2006	4	10	23.51	70.06	4.9	4.9	4.9	Banni <sup>a</sup>	
11	2006	6	12	23.88	70.43	27.3	4.4		Gedi/Is. Belt F.	
12	2007	5	13	23.44	70.42	20.4	4.7		South Wagad F.	
13	2007	5	24	23.298	70.026	9.0	4.1		Kachchh Mainland F.	Thrust
14	2007	10	8	23.295	70.075	9.6	4.7	4.5	Kachchh Mainland F.	Left Lateral
15	2008	3	9	23.396	70.359	18.5	4.9	4.5	South Wagad F.	Left Lateral
16	2009	10	28	23.71	69.91	8.5	4.4	4.4	Gora Dungar F.	Left Lateral
17	2011	5	17	23.55	70.57	18.2	4.2		E. of North Wagad F.	Thrust
18	2011	8	13	23.45	70.40	22.2	4.5	4.3	South Wagad F.	
19	2012	4	14	23.39	70.54	19	4.1	4.0	South Wagad F.	
20	2012	6	19	23.65	70.28	11	5.0	5.0	Khadir Tr. F.	
21	2012	12	8	23.13	70.42	21	4.5	4.1	20 km SSE of Bhachau Kandla <sup>b</sup>	
22	2013	3	30	23.56	70.38	24	4.5		Chobari <sup>a</sup>	

<sup>a</sup> Adapted from Rastogi et al. (2014)

## 7 Conclusions

This study complements some earlier observations (Talwani 2014), leading to the following conclusions regarding the nature of IPEs; specifically those in continental regions and associated with old rift structures. IPEs occur in response to local stress buildups on geological features, identified as local stress concentrators. When the magnitude of the temporal buildup of the local stress,  $S_L$ , approaches that of the regional stress,  $S_T$ , IPEs result. This buildup of  $S_L$  and its interaction with  $S_T$  can result in a detectable rotation of the latter over regions with wavelengths as small as tens of kilometers. Due to low tectonic strains in intraplate regions, larger stress drops associated with IPEs, and the availability of multiple, suitable LSCs, IPEs tend not to reoccur at earlier epicenters, but “roam” to newer structures, preferentially within rifts. The observation of roaming, non-repeat IPEs has direct consequence on identifying future locations of IPEs, and accurate assessment of seismic hazards posed by them. A possible correlation of anomalous ground movement and seismicity in Kutch points to the need for new strategies in monitoring ground motion in intraplate regions. These features are discussed below.

### 7.1 Mechanical basis for preferred location of IPEs in rifts

Intracratonic rifts form by extension in response to plate margin processes, with the resulting geometry a series of half-grabens separated by accommodation zones (Ziegler 1987). The term “basin inversion” is used to describe the tectonic process in which deep parts of a sedimentary basin or continental rift reverses its vertical direction of movement and becomes uplifted (Ziegler 1987). Among different intraplate discontinuities within the rigid crust, rifts with a thinner crust are most prone to inversion in response to compressional stresses emanating from plate boundaries (Ziegler 1987).

Hansen and Nielsen (2003) developed a continuum model to investigate the whole sequence of lithospheric rifting and subsequent basin reactivation and inversion by compression. During the rifting process boundary faults and interior conjugate faults extending to the brittle-ductile transition developed, together with rift pillows. On the

application of compressional stresses basin inversion followed as a natural consequence. The inversion preferentially utilized the inherited zones of crustal weakness. Compressive strains were preferentially located along the boundary faults, interior through-going and conjugate faults and on top of the up-welled mantle in the lower crust. These structures within the rift were the locations of large strains and sites for future earthquakes. Thus, modeling and field observations attest to conclusion that the preferential location of IPEs in old rifts has a mechanical basis.

### 7.2 Local stress concentrators and stress rotation

While plate boundary earthquakes are associated with well-defined faults, IPEs are associated with a diverse variety of LSCs. Of the various LSCs (fault bends, fault intersections, rift pillows, shallow plutons, etc.) favorably oriented (relative to  $S_T$ ) restraining stepovers provide locations for the largest stress build up and are the hosts of the larger IPEs.

The stress interaction between  $S_T$  and  $S_L$ , also can result in the local rotation of the observed ambient (final) stress  $S_F$ . The angle of rotation depends on the magnitude and direction of  $S_L$ , which in turn depends on its temporal history, the nature of the LSC, and its geometrical relationship with  $S_T$ . Thus, the directions of  $S_L$  associated with two neighboring LSCs a few kilometers apart, with different geometries can be different, such that the direction of  $S_F$  at the two locations can differ by tens of degrees. Such a large difference in directions of the local stress fields has been observed in the NW and SE clusters of seismicity in the Charlevoix seismic zone, located ~15 km apart, and in the seismicity at and near (approx. tens of kilometers) the intersection of the Blytheville and Reelfoot faults in the NMSZ.

### 7.3 Non-repeat earthquakes

Two factors contribute to the observation of non-repeat earthquakes in intraplate regions. First, in contrast with plate boundaries where the tectonic strain rates are high, those in intraplate settings are ~two orders of magnitude lower.

A second factor contributing to this observation is the larger stress drop associated with IPEs compared with their plate boundary counterparts. Scholz et al. (1986)

compared the stress drops of large earthquakes and found that those for IPEs are systematically greater than those for interplate earthquakes by a factor of 6. These results were found independent of the focal mechanism types. With a larger data base, Allmann and Shearer (2009) found that the difference was by a factor of 2. Kato (2009) suggested that IPEs with larger stress drops are associated with spatially heterogeneous sliding behavior and loading process. In a model study, he assumed that for IPEs slip was confined to the structure (LSC ?) surrounded by a permanently locked area, whereas in the case of interplate earthquakes the seismogenic feature was surrounded by a creeping area. Combining these two observations, with the availability of different LSCs, explains the observation of “roaming” or non-repeat earthquakes. The stress buildup and release on different LSCs results in a sequence of earthquakes at different locations, rather than their recurrence on the same fault.

The observations of non-repeat earthquakes and paleo-seismic investigations show that IPE sequences (some with temporal clustering) are often separated by long periods of quiescence. This observation may explain the absence of historical or current seismicity on the Meers fault in southwestern Oklahoma, where paleo-seismic evidence suggests the occurrence of a major earthquake ~1200 to 1300 years BP (Crone and Luza 1990).

#### 7.4 Reconciling GPS and paleo-seismological observations in the NMSZ

In the NMSZ, GPS observations of very low continental strain rates of  $\sim 10^{-9}$  year<sup>-1</sup> (Newman et al. 1999) have been hard to reconcile with the recurrence rates of ~500 years for M 7 earthquakes, determined from paleo-seismological data (Calais and Stein 2009). The low strain rates determined from GPS data would imply a minimum repeat time of 10,000 years for low M 7 earthquakes (Calais and Stein 2009). The concepts of LSCs and non-repeat earthquakes offer a possible explanation. The current methods of calculating regional strain over hundreds of kilometers using several GPS receivers are not geared to detect localized pockets of elevated strain rates surrounding LSCs and are apt to miss them in regional strain rate measurements. Also the observation of non-repeat earthquakes suggests that after the stress release at a particular LSC, which hosted a recent earthquake, it is unlikely to be the location of

another large earthquake in a few centuries given the low continental strain rates, and given the availability of other LSCs where stresses have been accumulating for thousands of years. This scenario suggests that the availability of several LSCs within a broad seismic zone (hundreds of kilometers by hundreds of kilometers); characterized by low strain rates, detected by regional GPS observations; could explain the temporal clustering of large earthquakes, inferred from paleo-seismological investigations.

#### 7.5 Implications for seismic hazard evaluation

The observation of non-repeat earthquakes has some major implications. The current methods of probabilistic seismic hazard analysis are based on observations at plate boundaries. Two common assumptions are that the earthquakes occur on the same fault (stationarity) and that the maximum magnitude of the earthquake ( $M_{\text{Max}}$ ) depends on the fault length (or the rupture length). This lack of stationarity of the seismic source on a particular fault in an intraplate setting belies the basic assumption of stationarity in probabilistic seismic hazard estimation methodology. It also affects the estimates of recurrence rates. For example, the recurrence rate estimates for the New Madrid and Charleston seismic zones (~500 years) are based on the assumption that the same seismic source was responsible for the development of sand blows, within the broad seismic zones, at different times in the Late Holocene. These estimates may have to be modified if newer observations invalidate this assumption of stationarity.

Also for an IPE the magnitude of the stress buildup, and hence  $M_{\text{Max}}$ , depends on the nature of the LSC, e.g., the fault geometry for intersecting faults and stepovers, the size and density contrast for mass anomalies rather than only on the fault length for plate boundary earthquakes. These dichotomies require a reassessment of methods of seismic hazard estimation in intraplate settings and the development of new ones.

#### 7.6 Need for new strategies in monitoring of ground motion

The observations in Kutch also might shed some light on an ongoing debate. Two decades of GPS measurements in the NMSZ have failed to provide a consensus on whether there is any evidence of anomalous geodetic strain (see, e.g., Newman et al. 1999), a view

contradicted by Frankel et al. (2012). According to the initial observations in Kutch, we would expect to find local pockets of ground deformation in the vicinity of a LSC, which may not be detectable by the current field techniques which lack the necessary resolution and coverage.

These observations suggest that with further improvements in instrumentation, analysis techniques, and with detailed, focused, complementary seismological and geodetic measurements, it may become possible to routinely detect pre-seismic increases in local strain rates, whose detection may indicate potential locations of large and moderate earthquakes. A refocus of strain measurement strategy may be in order. For example, the deployment of a dense network of GPS receivers surrounding the intersection of the Blytheville and Reelfoot faults in the NMSZ may be productive. The preliminary finding at Kutch suggests that in intraplate regions where there is evidence of large-scale thrusting, regular InSAR observations may be fruitful in identifying potential LSCs.

The results of this study are initial steps in understanding the seismogenesis and nature of intraplate earthquakes. Additional field studies and theoretical modeling are needed to further confirm these ideas and to develop better models.

**Acknowledgments** My thanks to Tom Owens, Bill Clendenin, Don Stevenson, the anonymous reviewers, and the Editor for their comments and Ethan Anderson for help with the figures. A special thanks to B.K.Rastogi for discussions and Figures 4 and 6.

## References

- Agurto-Detzel H, Assumpção M, Bianchi M, Pirchiner M (2015) Intraplate seismicity in mid-plate South America: correlations with geophysical lithospheric parameters. In: Landgraf A, Kuebler S, Hintersberger E, Stein S (eds) Seismicity, fault rupture and earthquake hazards in slowly deforming regions., Geological Society of London, Special Publications, 432, doi: 10.1144/SP432.5
- Allmann BP, and Shearer PM (2009) Global variations of stress drop for moderate to large earthquakes. *J. Geophys. Res.* 114: doi:10.1029/2008JB005821
- Aki K (1979) Characterization of barriers on an earthquake fault. *J Geophys Res* 84:6140–6148
- Al-Shukri HJ, Lemmer RE, Mahdi HH, Connelly JB (2005) Spatial and temporal characteristics of paleoseismic features in the southern terminus of the New Madrid seismic zone in eastern Arkansas. *Seis Res Lett* 76:502–511
- Baird AF, McKinnon SD, Godin L (2010) Relationship between structures, stress and seismicity in the Charlevoix seismic zone revealed by 3-D geomechanical models: implications for the seismotectonics of continental interiors. *J Geophys Res* 115. doi:10.1029/2010JB007521
- Baroux E, Béthoux N, Bellier O (2001) Analysis of the stress field in southeastern France from earthquake focal mechanisms. *Geophys J Int* 145:336–348
- Bisht RS (2011) Major earthquake occurrences in Archaeological Strata of Harappan Settlement at Dholavira (Kachchh, Gujarat). In: Proceedings of International Symposium on the 2001 Bhuj earthquake and advances in Earthquake Science-AES 2011, ISR, Gandhinagar, 112
- Biswas SK (2005) A review of structure and tectonics of Kutch basin, western India, with special reference to earthquakes. *Current Science* 88:1592–1600
- Biswas SK, Khattri KN (2003) Structure and tectonics of Kutch Basin, Western India, with special reference to earthquakes. *Journal of Geological Society of India* 61:626–629
- Bowman JR (1992) The 1998 Tennant Creek, Northern Territory, earthquakes: a synthesis. *Australian Journal of Earth Sciences* 39:651–669
- Calais E, Stein S (2009) Space geodetic evidence for time-variable deformation in the New Madrid seismic zone. *Science*, 323, 10.1126/science.1168122
- Calais E, Freed AM, Van Arsdale R, Stein S (2010) Triggering of New Madrid seismicity by Late-Pleistocene erosion. *Nature* 466:608–611
- Campbell DL (1978) Investigation of the stress-concentration mechanism for intraplate earthquakes. *Geophys Res Lett* 5: 477–479
- Clark D, McPherson A, Allen T (2014) Intraplate earthquakes in Australia. In: Talwani P (ed) Intraplate earthquakes. Cambridge University Press, Cambridge, pp 8–49
- Crone AJ, Luza KV (1990) Style and timing of Holocene faulting on the Meers fault, southwestern Oklahoma. *Geol Soc Am Bull* 102:1–17
- Csontos R, Van Arsdale R (2008) New Madrid seismic zone fault geometry. *Geosphere* 4:802–813
- Durá-Gómez I, Talwani P (2009) Finding faults in the Charleston area, South Carolina. 1. Seismicity data. *Seismological Research Letters* 80:883–900
- Durá-Gómez I, Talwani P (2010) Hydrodynamics of Koyna-Warna region, India. *Pure Appl Geophys* 167:183–213
- Frankel A, Smalley R, Paul J (2012) Significant motions between GPS sites in the New Madrid region: implications for seismic hazard. *Bull Seis Soc Am* 102:479–489
- Gangopadhyay A, Talwani P (2007) Two-dimensional numerical modeling suggests preferred geometry of intersecting faults. In: Stein S, Mazzotti S (eds) Continental intraplate earthquakes; science, hazard and policy issues, vol 425, *Geol. Soc. Am. Special Paper.*, pp 87–99. doi:10.1130/2007.2425(07)
- Gangopadhyay A, Dickerson J, Talwani P (2004) A two-dimensional numerical model for current seismicity in the New Madrid Seismic Zone. *Seis. Res Lett* 75:406–418
- Garner JT (1998) Re-evaluation of the seismotectonics of the Charleston, South Carolina area. MS thesis, University of South Carolina, Columbia, 250 pp
- Gomberg J, Ellis M (1994) Topography and tectonics of the central New Madrid seismic zone: results of numerical experiments

- using three dimensional boundary elements program. *Journal of Geophysical Research* 89:20,299–20,310
- Grana JP, Richardson RM (1996) Tectonic stress within the New Madrid seismic zone. *J Geophys Res* 101:5445–5458
- Hansen DL, Nielsen SB (2003) Why rifts invert in compression. *Tectonophysics* 373:5–24
- Haxby WF, Turcotte DL (1976) Stresses induced by the addition or removal of overburden and associated thermal effects. *Geology* 4:181–184
- Heidbach O, Tingay M, Barth A, Reinecker J, Kurfelß D, Müller B (2010) Global crustal stress pattern based on the World Stress Map database release 2008. *Tectonophysics* 482:3–15
- Hickman S, Sibson R, Bruhn R (1995) Introduction to special section: mechanical involvement of fluids in faulting. *J Geophys Res* 100:12,831–12,840
- Hildenbrand TG, Ravat D (1997) Geophysical setting of the Wabash Valley fault system. *Seismological Research Letters* 68:567–585
- Horton SP, Kim W-Y, Withers M (2005) The 6 June 2003 Bardwell, Kentucky earthquake sequence: evidence for a locally perturbed stress field in the Mississippi embayment. *Bull Seis Soc Am* 95:431–445
- Hurd O, Zoback MD (2012a) Regional stress orientations and stress compatibility of earthquake focal planes in the New Madrid seismic zone. *Seis Res Lett* 83:672–679
- Hurd O, Zoback MD (2012b) Intraplate earthquakes, regional stress and fault mechanics in the central and eastern U.S. and southeastern Canada. *Tectonophysics* 581:182–192
- Iio Y, Sagiya T, Kobayashi Y (2004) What controls the occurrence of shallow intraplate earthquakes? *Earth Planets Space* 56: 1077–1086
- Jaeger JC, Cook NGW (1979) *Fundamentals of rock mechanics*, 3. Chapman and Hall, London, p 591
- Johnston AC, Kanter LR (1990) Earthquakes in stable continental crust. *Sci Am* 262:68–75
- Johnson GA, Horton SP, Withers M, Cox R (2014) Earthquake focal mechanisms in the New Madrid seismic zone. *Seismological Research Letters* 85:257–267
- Jones TD, Gibson G, McCue KF, Denham D, Gregson PJ, Bowman JR (1991) Three large intraplate earthquakes near Tennant Creek, Northern Territory, on January 22, 1988. *BMR Jour Australian Geology and Geophysics* 12:339–343
- Kato A (2014) Intraplate earthquakes induced by reactivation of buried ancient rift system along the eastern margin of the Japan Sea. In: Talwani P (ed) *Intraplate earthquakes*. Cambridge University Press, Cambridge, pp 231–256
- Kato A, Sakai S, Hirata N et al (2006) Imaging the seismic structure and stress field in the source region of the 2004 mid-Niigata Prefecture earthquake: structural zones of weakness, seismogenic stress concentration by ductile flow. *Journal of Geophysical Research* 111:B08308. doi:10.1029/2005JB004016
- Kato N (2009) A possible explanation for difference in stress drop between intraplate and interplate earthquakes. *Geophys Res Lett* 36:L233311. doi:10.1029/2009GL040985
- Kawanishi R, Iio Y, Yukutake Y, Shibutani T, Kato H (2009) Local stress concentration in the seismic belt along Japan Sea coast inferred from precise focal mechanisms: Implications for the stress accumulation process on intraplate faults. *J. Geophys. Res* 114. doi:10.1029/2008JB005765
- Kenner SJ, Segall PA (2000) A mechanical model for intraplate earthquakes: application to the New Madrid seismic zone. *Science* 289:2329–2332
- King GCP (1986) Speculations on the geometry of the initiation and termination process of earthquake rupture and its relation to morphological and geological structure. *Pageoph* 124: 567–585
- Langenheim VE, Hildenbrand TG (1997) Commerce geophysical lineament-Its source, geometry, and relation to the Reelfoot rift and New Madrid seismic zone. *Geological Society of America Bulletin* 109:580–595
- Liu L, Zoback MD (1997) Lithospheric strength and intraplate seismicity in the New Madrid seismic zone. *Tectonics* 16: 585–595
- Liu M, Stein S, Wang H (2011) 2000 years of migrating earthquakes in north China: how earthquakes in midcontinents differ from those at plate boundaries. *Lithosphere* 3:128–132
- Liu M, Wang H, Ye J, Jia C (2014) *Intraplate earthquakes in North China*. In: Talwani P (ed) *Intraplate earthquakes*. Cambridge University Press, Cambridge, pp 97–125
- Long LT (1976) Speculations concerning southeastern earthquakes, mafic intrusions, gravity anomalies and stress amplification. *Earthquake Notes* 47:29–35
- Mandal P (2013) Seismogenesis of the uninterrupted occurrence of the aftershock activity in the 2001 Bhuj earthquake zone, Gujarat, India, during 2001–2010. *Nat Hazards* 65:1063–1083
- Mazarbaud Y, Béthoux N, Guilbert J, Bellier O (2005) Evidence for short-scale stress field variations within intraplate central-western France. *Geophys J Intl* 160:161–178
- Mazzotti S (2007) Geodynamic models for earthquake studies in intraplate North America. In: Stein S, Mazzotti S (eds) *Continental intraplate earthquakes; science, hazard and policy issues*, vol 425, *Geol. Soc. Am. Special Paper.*, pp 17–33. doi:10.1130/2007.2425(02)
- Mazzotti S, Townend J (2010) State of stress in central and eastern North America seismic zones. *Lithosphere* 2:76–83
- McClay K, Bonora M (2001) Analog models of restraining stopovers in strike-slip fault systems. *American Association of Petroleum Geologists Bulletin* 85:233–260
- Mooney WD, Ritsema J, Hwang YK (2012) Crustal seismicity and earthquakes catalog maximum moment magnitude ( $M_{\text{cmax}}$ ) in stable continental regions (SCRs): Correlation with the seismic velocity of the lithosphere. *Earth and Planetary Sc Letters* 357–358:78–83
- Munson PJ, Obermeier SM, Munson CA, Hajic ER (1997) Liquefaction evidence for Holocene and latest Pleistocene in the southern halves of Indiana and Illinois—a preliminary overview. *Seismological Research Letters* 68:523–536
- Nábělek J, Chen WP, Ye H (1987) The Tangshan earthquake sequence and its implications for the evolution of the North China basin. *Jour Geophysical Research* 92:12615–12628
- Newman A, Stein S, Weber J, Engeln J, Mao A, Dixon T (1999) Slow deformation and lower seismic hazard at the New Madrid seismic zone. *Science* 284:619–621
- Pollitz FF, Kellogg L, Burgmann R (2001) Sinking mafic body in a reactivated lower crust: a mechanism for stress concentration at the New Madrid seismic zone. *Bull Seis Soc Am* 91:1882–1897
- Powell CA, Withers MM, Cox RT, Vlahovic G, Arroucau P (2014) Crustal velocity structure associated with the eastern Tennessee seismic zone:  $V_p$  and  $V_s$  images based upon local

- earthquake tomography. *J. Geophys. Res. Solid Earth*, 119, doi:10.1002/2013JB010433
- Powell CA (2015) Crustal structure below the Southern Appalachian Blue Ridge and Valley and ridge provinces: implications for national seismic hazard maps. *Abstract Seis Res Letters* 86(2B):598
- Pratt TL (2012) Kinematics of the New Madrid seismic zone, central U. S., based on stepover models. *Geology* 40:371–374
- Rajendran CP, Rajendran K (2001) Characteristics of deformation and past seismicity associated with the 1819 Kutch earthquake, northwestern India. *Bull Seis Soc Am* 91:407–426
- Rastogi BK, Choudhury P, Dumka R, Sreejith KM, Majumdar TJ (2012) Stress pulse migration by viscoelastic process for long-distance delayed triggering of shocks in Gujarat, India, after the 2001 Mw 7.7 Bhuj earthquake. In: Sharma AS, Bundle A, Dimri VP, Baker DN (eds) *Extreme events and natural hazards: the complexity perspective*, *Geophys. Monogr. Ser. v. 196*. AGU, Washington, pp 63–73. doi:10.1029/GM196
- Rastogi BK, Mandal P, Biswas SK (2014) Seismogenesis of earthquakes occurring in the ancient rift basin of Kachchh, Western India. In: Talwani P (ed) *Intraplate earthquakes*. Cambridge University Press, Cambridge, pp 126–161
- Reddy CD, Patil PS (2008) Post-seismic crustal deformation and strain rate in Bhuj region, Western India, after the 2001 January 26 earthquake. *Geophys J Intl* 172:593–606
- Reiter K, Heidbach O, Schmitt D, Haug H, Ziegler M, Moeck I (2014) A revised crustal stress orientation database for Canada. *Tectonophysics* 636:111–124
- Russ DP (1982) Style and significance of surface deformation in the vicinity of New Madrid, Missouri, Investigations of the New Madrid, Missouri, earthquake region. *US Geological Survey Professional Paper* 1236:95–114
- Sandiford M, Egholm DL (2008) Enhanced intraplate seismicity along continental margins. Some causes and consequences. *Tectonophysics* 457:197–208
- Scholz CH (1977) A physical interpretation of the Haicheng earthquake prediction. *Nature* 267:121–124
- Scholz CH, Aviles CA, Wesnousky SG (1986) Scaling differences between large interplate and intraplate earthquakes. *Bull Seis Soc Am* 76:65–70
- Schulte S, Mooney W (2005) An updated global earthquake catalogue for stable continental regions: reassessing the correlation with ancient rifts. *Geophys J Int* 161:707–721
- Schweig E, Ellis MA (1994) Reconciling short recurrence intervals with minor deformation in the New Madrid seismic zone. *Science* 264:1308–1311. doi:10.1126/science.264.5163.1308
- Segall P, Pollard DD (1980) Mechanics of discontinuous faults. *Journal of Geophysical Research* 85:4,337–4,350
- Shedlock KM, Baranowski J, Weiwan X, Liang HX (1987) The Tangshan aftershock sequence. *Jour Geophysical Research* 92:2791–2803
- Sibson RH (1986) Rupture interaction with fault jogs. In: Das S, Boatwright J, Scholz CH (eds) *Earthquake source mechanics*. AGU Geophysical Monograph 37, Maurice Ewing Series 6, American Geophysical Union, Washington, DC, pp 157–167
- Sonder LJ (1990) Effects of density contrasts on the orientation of stress in the lithosphere: relation to principal stress directions in the Transverse Ranges, California. *Tectonics* 9:761–771
- Steffen R, Eaton WP (2012) Moment tensors, state of stress and their relation to post-glacial rebound in northeastern Canada. *Geophys J Intl* 189:1741–1752
- Stein S, Sleep N, Geller RJ, Wang SC, Kroeger C (1979) Earthquakes along the passive margin of eastern Canada. *Geoph Res Lett* 6:537–540
- Sykes LR (1978) Intra-plate seismicity, reactivation of pre-existing zones of weakness, alkaline magmatism, and other tectonics post-dating continental separation. *Reviews of Geophysics and Space Physics* 16:621–688
- Talwani P (1981) Earthquake prediction studies in South Carolina. In: Simpson DW, Richards PG (eds) *Earthquake prediction. An international review*, Maurice Ewing Series 4, American Geophysical Union, Washington, DC, pp 381–394
- Talwani P (1988) The intersection model for intraplate earthquakes. *Seis Res Lett* 59:305–310
- Talwani P (1999) Fault geometry and earthquakes in continental interiors. *Tectonophysics* 305:371–379
- Talwani P (2014) A unified model for intraplate earthquakes. In: Talwani P (ed) *Intraplate earthquakes*. Cambridge University Press, Cambridge, pp 275–302
- Talwani P, Durá-Gómez I (2009) Finding faults in the Charleston area, South Carolina. 2. Complementary data. *Seismological Research Letters* 80:901–919
- Talwani P, Schaeffer WT (2001) Recurrence rates of large earthquakes in the south Carolina Coastal Plain based on paleoliquefaction data. *J Geophys Res* 106:6621–6642
- Tremblay A, Long B, Masse M (2003) Supracrustal faults of the St. Lawrence rift system, Quebec: kinematics and geometry as revealed by field mapping and marine seismic reflection data. *Tectonophysics* 369:231–252
- Tuttle MP, Schweig ES, Sims JD, Lafferty RH, Wolf LW, Haynes ML (2002) The earthquake potential of the New Madrid seismic zone. *Bull Seis Soc Am* 92:2080–2089
- Tuttle MP, Schweig ES, Campbell J, Thomas PM, Sims JD, Lafferty RH (2005) Evidence for New Madrid earthquakes in A.D. 300 and 2350 B.C. *Seis Soc Res Lett* 76:489–501
- Wallace K, Bilham R, Blume F, Gaur VK, Gahalaut V (2006) Geodetic constraints on the Bhuj 2001 earthquake and surface deformation in the Kachchh Rift Basin. *Geophysical Research Lett* 33:L10301. doi:10.1029/2006GL025775
- Wang CY, Zhang XK, Lin ZY, Wu QJ, Zhang YS (1997) Crustal structure beneath the Xingtai earthquake area in North China and its tectonic implication. *Tectonophysics* 274:307–319
- Wang XB, Ma J, Liu LQ (2013) Numerical simulation of large shear strain drops during jog failure for echelon faults based on heterogeneous and strain-softening model. *Tectonophysics* 608:667–684
- Ziegler PA (1987) Late Cretaceous and Cenozoic intra-plate compressional deformations in the Alpine foreland—a geodynamic model. *Tectonophysics* 137:389–420
- Zoback MD et al (1993) Upper-crustal strength inferred from stress measurements to 6 km depth in the KTB borehole. *Nature* 365:633–635
- Zoback ML (1992) First- and second order patterns of stress in the lithosphere: the world stress map project. *J Geophys Res* 97(11):703–11,728
- Zoback ML, Richardson RM (1996) Stress perturbation associated with the Amazonas and other ancient continental rifts. *J Geophys Res* 101:5459–5475